Environment-Independent SNR Measurement Method for Underwater Acoustic Communication Systems

SHINGO YOSHIZAWA
Faculty of Engineering,
Kitami Institute of Technology,
Koen-Cho 165, Kitami, 090-8507,
JAPAN

Abstract: - Underwater acoustic communication (UAC) is used as a means of long-range communication for autonomous underwater vehicles (AUVs) and underwater wireless sensor networks (UWSNs). The signal-to-noise ratio (SNR) is an important metric for predicting the communication range and transmission rate in UAC systems. The SNR measurements of input SNR (ISNR) and output SNR (OSNR) are widely used in acoustic modems. However, they are sensitive to acoustic reflections, and their measured values depend on the communication environment. This paper presents a pure carrier-to-noise ratio (PCNR) method that extracts only signal power derived from sound propagation loss. This method enables environment-independent SNR measurements. The effectiveness of the proposed method is verified through simulations and experiments conducted in a water tank.

Key-Words: - Underwater acoustic communication, signal-to-noise ratio, carrier-to-noise ratio, impulse response, cross-correlation, line-of-sight, non-line-of-sight

Received: March 9, 2026. Revised: May 2, 2026. Accepted: June 2, 2026. Published: July 21, 2026.

1 Introduction

Underwater acoustic communication (UAC) is used as a means of long-range communication for autonomous underwater vehicles (AUVs) [1] and underwater wireless sensor networks (UWSNs) [2]. UAC has been studied for a long time, as well as radio communication. For example, single sideband amplitude modulation (SSB-AM) communication units were developed in the 1950s. Digital modulation schemes such as spread spectrum [3], OFDM [4], and MIMO [5] are often discussed in current UAC systems. Spread-spectrum (SS) is widely used for long-distance transmission [6]. In our previous work, we presented a digital modem scheme called stretchable symbols with multiple sequences (SSMS) [7] to combat with non-uniform Doppler shifts.

The signal-to-noise ratio (SNR) measurement is important for predicting the communication range and transmission rate in UAC systems. In underwater acoustic modems, a received signal strength indicator (RSSI) is typically measured, where the SNR value is obtained by subtracting the noise strength from the RSSI. Transmit power control and data rate adjustment are performed according to the measured SNR.

Although the SNR is defined as the ratio of signal power to background noise power, there are various methods for SNR measurement. The input SNR (ISNR) measures the signal and noise power values of the received signal [8]. The output SNR (OSNR) is defined as the ratio of the average power of the demodulated message signal to the average power of the noise [9]. The SNR estimation methods based on ISNR and the OSNR have been discussed in [10].

The conventional methods are sensitive to acoustic reflections. When there are many reflections of acoustic waves from the surroundings, the ISNR value increases. Even with a high ISNR, the communication condition may deteriorate due to multipath interference. As long as channel estimation and equalization are perfect, the OSNR plays the role of an accurate SNR indicator. However, the OSNR value depends on the demodulation quality after the equalization.

This paper presents a pure carrier-to-noise ratio (PCNR) method that extracts only signal power from sound propagation loss to achieve an environment-independent SNR measurement. The CNR is one of the SNR metrics and is defined as the ratio of the received modulated carrier signal power. The PCNR is calculated by the cross-correlation function between the received signal and the reference signal. It is a stable metric that is insensitive to acoustic reflections. The effectiveness of the proposed method is verified through simulations and experiments conducted in a water tank.

2 System Model

The block diagram of the SNR measurement in UAC systems is shown in Figure 1. Although this paper does not restrict the communication system, we explain the case of phase shift keying (PSK) modulation for simplicity. When the input data is mapped to a PSK symbol, the transmitted signal is modeled as

$$x(t) = \Phi_d(t)e^{\mathrm{j}\omega_c t}, \tag{1}$$

where t is a discrete time index and $\Phi_d(t)$ is a baseband PSK signal for the d-th symbol. The PSK signal is modulated by the carrier signal $e^{\mathrm{j}\omega_c t}$.

The received signal after passing through the sound wave propagation path is expressed by

$$y(t) = h(t) * x(t) + n(t), \tag{2}$$

where $h(t)$ is an impulse response from a transmitter to a receiver, $n(t)$ is a noise component, and $*$ shows a convolution operation.

If all signal components are known, the theoretical SNR can be computed as

$$\xi_{\mathrm{SNR}} = \frac{E\{|h(\tau_0)*x(t)|^2\}}{E\{|n(t)|^2\}} \approx \frac{E\{|h(\tau_0)|^2\}}{E\{|n(t)|^2\}}, \tag{3}$$

where the amplitude of the transmitted signal is adjusted as $|x(t)| \approx 1$. The theoretical SNR is defined by the received signal power in the direct path and the noise power. The impulse response for only the direct path is expressed as

$$h(\tau_0) = \alpha, \tag{4}$$

where α is the signal attenuation coefficient when an acoustic wave propagates from a transmitter to a receiver. The value of α is one when there is no propagation loss.

In actual UAC systems, the signal components of $h(0)$ and $n(t)$ are unknown. The SNR value is measured from the received signal, and the various measurement methods have been discussed.

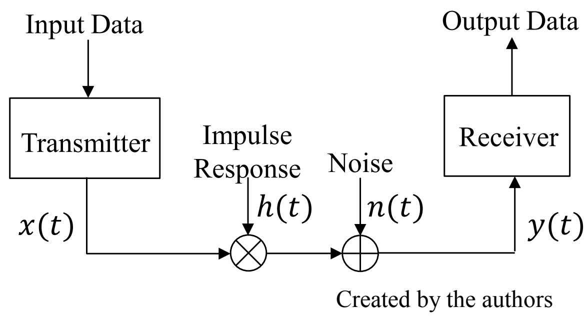

Fig. 1: Block diagram of SNR measurement in UAC systems.

3 Conventional Methods

3.1 Input SNR

The ISNR measures the signal and noise power values of the received signal in the time domain. The ISNR measurement portions in a communication frame are illustrated in Figure 2. The frame format commonly used in UAC systems consists of a preamble and data symbols. The signal portion $y_{\mathrm{S}}(t)$ is extracted from the preamble. The noise portion $y_{\mathrm{N}}(t)$ It is located between frames. The ISNR is computed as

$$\xi_{\mathrm{ISNR}} = \frac{E\{|y_{\mathrm{S}}(t)|^2\} - E\{|y_{\mathrm{N}}(t)|^2\}}{E\{|y_{\mathrm{N}}(t)|^2\}}. \tag{5}$$

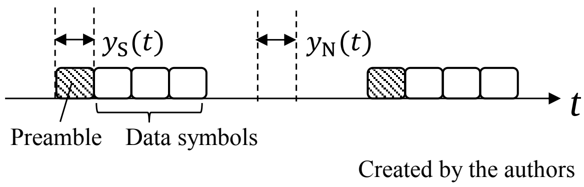

Fig. 2: ISNR measurement portions in the communication frame.

3.2 Output SNR

The OSNR is defined as the ratio of the average power of the demodulated message signal to that of the noise. The OSNR is computed as

$$\xi_{\mathrm{OSNR}} = \frac{E\{|\Phi_d(t)|^2\}}{E\{|\hat{\Phi}_d(t) - \Phi_d(t)|^2\}}, \tag{6}$$

where $\hat{\Phi}_d(t)$ is the baseband PSK signal after the demodulation at the receiver side. Examples of the baseband PSK signals at the transmitter and receiver sides are plotted in Figure 3. The noise component is obtained by the difference between the two signals.

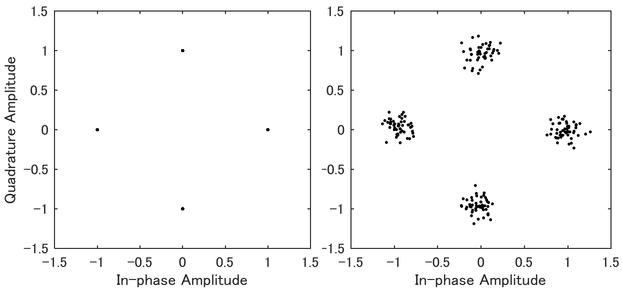

(a) $\Phi_d(t)$ at transmitter side (b) $\widehat{\Phi}_d(t)$ at receiver side

Created by the authors

Fig. 3: Examples of baseband PSK signals.

3.3 Influence of acoustic reflections

We investigated the influence of acoustic reflections using an acoustic simulator. The simulator tracks sound waves using sound ray tracing. Based on the path that sound waves take from a sound source to a receiver, it generates an impulse response is generated. Users specify the sound field space, sound pressure reflectance, and the positions of the sound source and receiver in the simulator [11].

Figure 4 shows an example of acoustic rays, where the parameters of $\boldsymbol{R} = [R_{\mathrm{x1}}, R_{\mathrm{x2}}, R_{\mathrm{y1}}, R_{\mathrm{y2}}, R_{\mathrm{z1}}, R_{\mathrm{z2}}]$ give the sound pressure reflectance ratios on the six surfaces. When the reflectance ratios are set to $[0, 0, 0, 0, 0.7, 1]$, The sound waves are reflected many times on the top and bottom surfaces.

Figure 5 shows an example of the impulse response. The first peak is caused by the direct path, while the other peaks are caused by the reflected paths. In this figure, the signal attenuation coefficient is given by $h(\tau_0) = 0.1$. This indicates that the amplitude of the transmitted signal is attenuated to one-tenth by the direct path from the transmitter to the receiver.

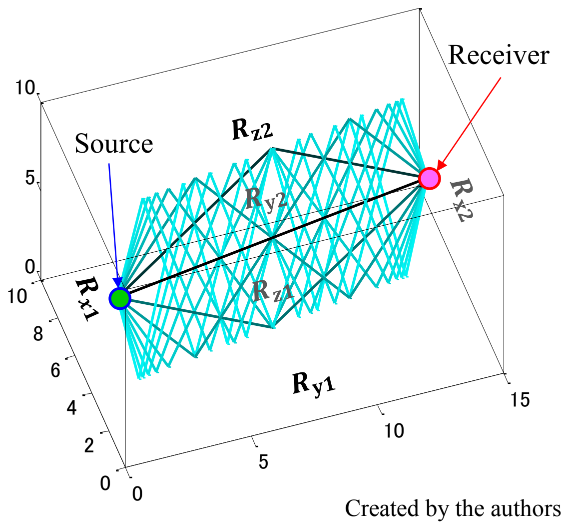

Created by the authors

Fig. 4: Example of acoustic rays in an acoustic simulator.

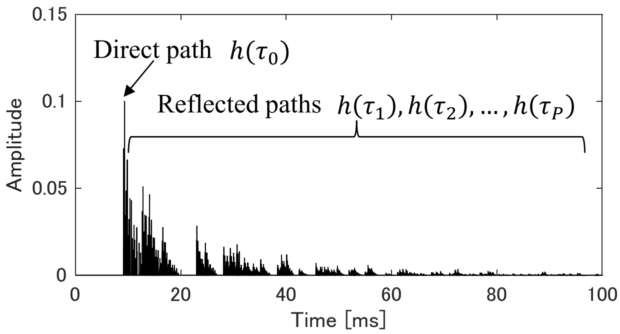

Created by the authors

Fig. 5: Example of impulse response in acoustic simulator.

Figure 6 shows the ISNR measurement results for a theoretical SNR of 10 dB for three acoustic reflection conditions, where the acoustic rays and the received signals are plotted. In Figure 6(a), which shows no reflection, the ISNR value is equal to the theoretical SNR value. When the water surface reflection is added as shown in Figure 6(b), the ISNR value increases slightly. With reflections from all boundary surfaces, the ISNR value is 16.9 dB in Figure 6(c), where significant differences are observed between the ISNR and SNR values.

Acoustic rays Received signal

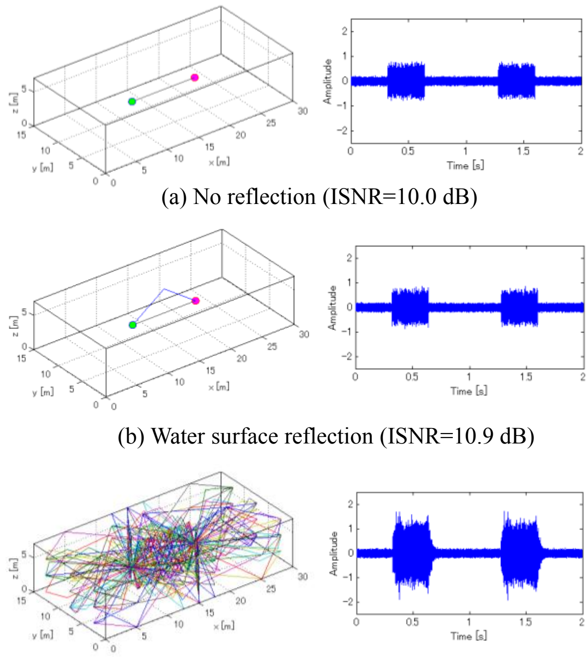

(a) No reflection (ISNR=10.0 dB)

(b) Water surface reflection (ISNR=10.9 dB)

(c) Reflections from all boundary surfaces (ISNR=16.9 dB)

Created by the authors

Fig. 6: ISNR measurement results under three acoustic reflection conditions.

The amplitude of the signal portion $y_S(t)$ increases under conditions of strong acoustic reflection. This amplitude increase is caused by $h(\tau_1)$, $h(\tau_2)$, ..., and $h(\tau_P)$. This phenomenon implies that the ISNR is sensitive to the acoustic reflections.

Figure 7 shows the OSNR measurement results without and with phase and amplitude offsets for a theoretical SNR of −5 dB. The red triangles indicate the transmitted baseband signals. The preamble part in Figure 2 is treated as known at the receiver side and is used for channel estimation and equalization. The phase and amplitude offsets are compensated in the demodulation process. However, this compensation is not always perfect. The OSNR values differ significantly with and without residual phase and amplitude offsets. In Figure 7, the OSNR values are 19.8 dB and 11.0 dB, respectively, despite the noise component having the same magnitude. The OSNR value depends on the demodulation quality after the equalization.

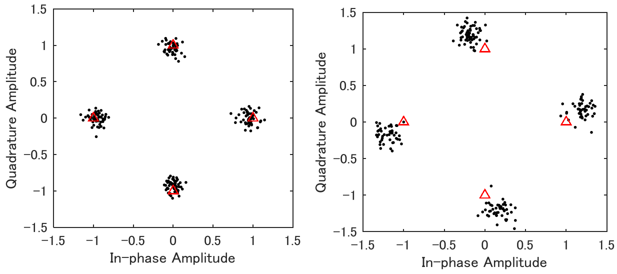

(a) Without phase and amplitude offsets (OSNR = 19.8 dB)

(b) With phase and amplitude offsets (OSNR = 11.0 dB)

Created by the authors

Fig. 7: OSNR measurement results without and with phase and amplitude offsets.

4 Proposed Method

We focus on the cross-correlation between the received signal and the local template signal for the SNR measurement. In wireless communication, the preamble shown in Figure 2 is commonly used for the SNR estimation [11]. When a part of the transmitted signal $x(t)$ is known by the preamble, the cross-correlation between the received signal and the preamble can be expressed as follows:

$$\begin{aligned}\gamma(t) &= y(t) \star x(t)\\ &= (h(t) * x(t) + n(t)) \star x(t)\\ &= h(t) * x(t) \star x(t) + n(t) \star x(t)\\ &= h(\tau_0) + h(\tau_1) + \ldots + h(\tau_P) + \tilde{n}(t),\end{aligned} \quad (7)$$

where $\star$ denotes the operation of cross-correlation. The SNR based on the cross-correlation is calculated as

$$\xi_{\mathrm{Corr}} = \frac{|h(\tau_0)|^2}{E[|\gamma(t)|^2]}, \quad (8)$$

where $E[\,]$ denotes the expected value.

The measured cross-correlation corresponds to the impulse response under noisy conditions, as illustrated in Figure 8. The magnitude of the impulse response at the direct path $h(\tau_0)$ can be extracted using the maximum peak detection as $|h(\tau_0)| = \max[|\gamma(t)|]$. The noise power can be measured from the other components. However, this SNR metric is affected by the acoustic reflections because the direct path and the reflected path cannot be separated in the cross-correction function of $\gamma(t)$.

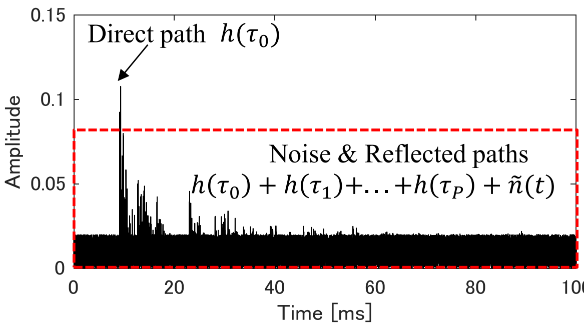

Created by the authors

Fig. 8: Example of cross-correlation under noisy conditions.

We propose the PCNR method, the key idea of which is to separate the impulse response of the reflected paths $h(\tau_p)$ and noise component $\tilde{n}(t)$. The steps of the PCNR are described below:

Step 1:
Extract the received signal not only from the preamble portion but also from the section that includes the portion without the communication frame.

Step 2:
The template signal is the same length as the received signal, with zeros added after the preamble.

Step 3:
Perform a cross-correlation calculation between the received signal and the template signal using the FFT method.

Step 4:
Measure the signal power at the position with the maximum value. The noise power is measured from the section where no communication frame exists.

Figure 9 illustrates the timing charts of the proposed method. It is possible to extract the noise component and separate the impulse response at the reflected paths. The PCNR is calculated as follows:

$$\xi_{\mathrm{PCNR}} = \frac{|h(\tau_0)|^2}{L \cdot E[|\gamma_N(t)|^2]}, \tag{9}$$

where $\gamma_N(t)$ is the cross-correlation at the noise portion without the acoustic wave reflection, and L denotes the signal length in the cross-correlation analysis. The proposed method achieves an environment-independent SNR measurement that is not affected by acoustic reflections.

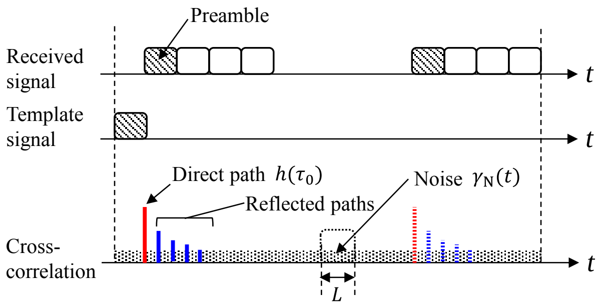

Created by the authors

Fig. 9: Timing charts of the proposed method.

5 Simulation Results

We compare the SNR measurement methods in a simulation under the three acoustic reflection conditions described in Section 3.3. SNR measurements are performed simultaneously with demodulation of the communication frame. The communication specifications are listed in Table 1. This evaluation uses a direct-sequence spread spectrum (DSSS) system. The SNR measurement results are shown in Figure 10. The theoretical SNR can be computed precisely in the simulation because the signal power and the noise power are known.

Table 1. Communication specifications.

Sampling frequency	250 kHz
Frequency band	12 kHz - 32 kHz
Primary modulation	QPSK
Secondary modulation	DSSS
Symbol length	16 ms
Number of symbols	100
Frame length	1.76 s
Inter-frame spacing	0.80 s
Number of bits per frame	200 bits
Transmit data rate	125 bps
Error correcting code	None
Channel equalization	One tap equalizer

Created by the authors

As shown in Figure 10(a), the SNR values of ISNR and PCNR are nearly identical to the theoretical SNR, except below −15 dB. In regions where the SNR is less than −15 dB, the signal power is very small, requiring long-term observation. The

OSNR does not match the theoretical SNR because the two metrics used to calculate them differ significantly.

Regarding the acoustic reflection conditions in Figure 10(b) and Figure 10(c), the ISNR does not provide accurate SNR values that align with the theoretical SNR values. Conversely, the PCNR achieves an environment-independent SNR measurement, meaning the measured SNR values are identical to the theoretical SNR values. The values of OSNR decrease as the acoustic reflection condition becomes more severe.

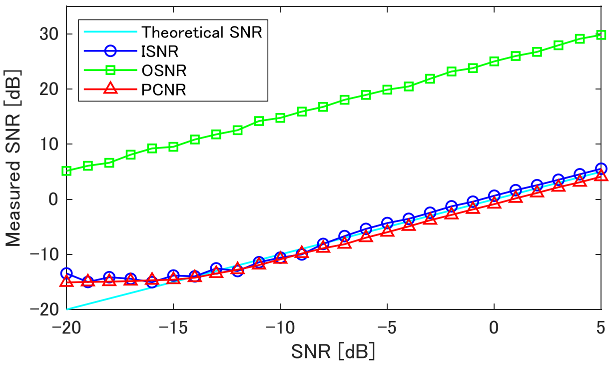

(a) No reflection

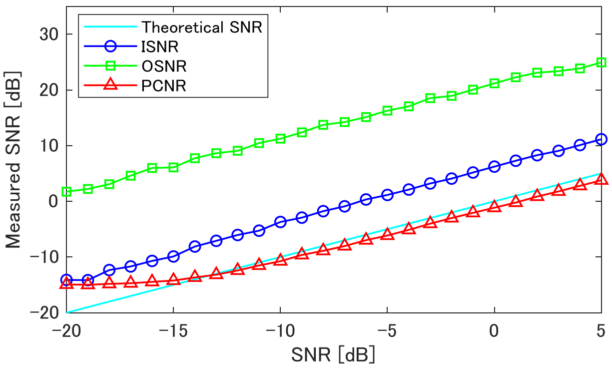

(b) Water surface reflection

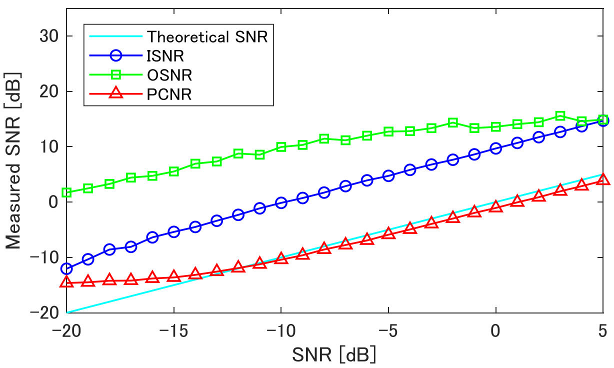

(c) Reflections from all boundary surfaces

Created by the authors

Fig. 10: SNR measurement results in simulation.

6 Experimental Results

The underwater acoustic experiment was conducted in a water tank. The size of the acoustic field is 21 × 21 × 3.3 meters (length, width, and height).

Figure 11 illustrates the locations of the transmitter and receiver hydrophones. The receiver hydrophone was fixed 1 m below the water surface. The transmitter hydrophone's location changes from 1 to 3 meters of water depth. This tank is stepped, and the depth changes from 1.5 m to 3.3 m. As the transmitter's position is lowered, the experimental condition changes from line-of-sight (LOS) to non-line-of-sight (NLOS). The NLOS condition causes significant sound propagation loss and degrades communication performance.

Figure 12 shows the SNR and BER measurement results. The horizontal axis indicates the transmitter hydrophone depth. While the ISNR value changes minimally with transmitter location, the BER worsens at depths greater than 2.5 m. The ISNR cannot detect this BER degradation. The PCNR value drops below 0 dB at depths greater than 2.5 m, indicating its ability to detect changes in communication conditions from LOS to NLOS. The PCNR is useful for observing sound propagation independently of acoustic reflection.

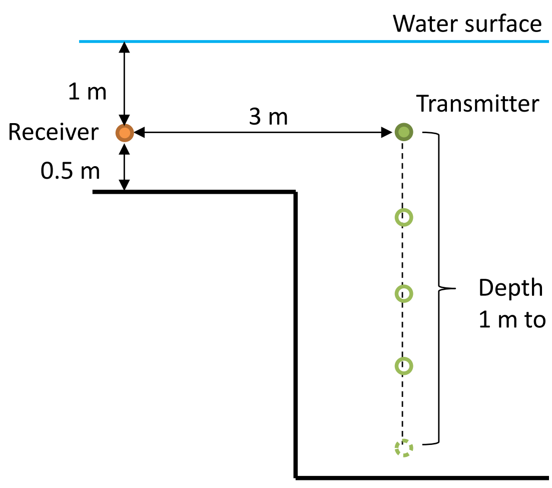

Created by the authors

Fig. 11: Locations of transmitter and receiver hydrophones in water tank.

7 Conclusion

This paper presented the PCNR method, which extracts signal power based solely on sound propagation loss. Through an evaluation of simulations and experiments, we confirmed that the PCNR method enables environment-independent SNR measurements, even in highly reflective conditions. In our future work, we will consider the applications of underwater acoustic networks for IoT communications [12].

Acknowledgement:
This work was supported by Safety and Security Technology Research and Promotion in Acquisition, Technology & Logistics Agency (ATLA), Japan (JPJ004596).

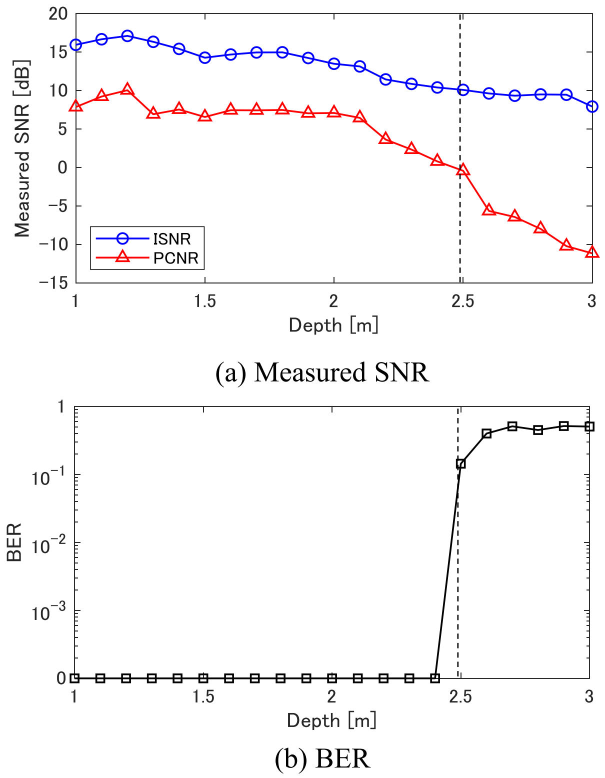

Created by the authors

Fig. 12: Experimental results.

Declaration of Generative AI and AI-assisted Technologies in the Writing Process

During the preparation of this work, the author used Grammarly and DeepL services in order to correct and improve the quality of English writing. After using this tool/service, the author reviewed and edited the content as needed and takes full responsibility for the content of the publication.

References:

[1] M. Jouhari, K. Ibrahimi, H. Tembine, J. Ben-Othman, "Underwater wireless sensor networks: a survey on enabling technologies, localization protocols, and internet of underwater things," IEEE Access, vol. 7, pp. 96879-96899, 2019, DOI: 10.1109/ACCESS.2019.2928876.

[2] Y. Yang, Y. Xiao, T. Li, "A survey of autonomous underwater vehicle formation: performance, formation control, and communication capability," IEEE Communications Surveys & Tutorials, vol. 23, no. 2, pp. 815-841, Feb. 2021, DOI: 10.1109/COMST.2021.3059998.

[3] F. Qu, X. Qin, L. Yang, T. C. Yang, "Spread-spectrum method using multiple sequences for underwater acoustic communications," IEEE Journal of Oceanic Engineering, vol. 43, no. 4, pp. 1215-1226, Oct. 2018, DOI: 10.1109/JOE.2017.2750298.

[4] M. Stojanovic, "Low complexity OFDM detector for underwater acoustic channels," IEEE OCEANS-Boston, pp. 1-6, Boston, USA, Sep. 2006, DOI: 10.1109/OCEANS.2006.307057.

[5] B. Li, J. Huang, S. Zhou, K. Ball, M. Stojanovic, L. Freitag, "MIMO-OFDM for high-rate underwater acoustic communications," IEEE Journal of Oceanic Engineering, vol. 34, no. 4, pp. 634-644, Oct. 2009, DOI: 10.1109/JOE.2009.2032005.

[6] Z. Liu, K. Yoo, T. C. Yang, S. E. Cho, H. C. Song, D. E. Ensberg, "Long-range double-differentially coded spread-spectrum acoustic communications with a towed array," IEEE Journal of Oceanic Engineering, vol. 39, no. 3, pp. 482-490, July 2014, DOI: 10.1109/JOE.2013.2264994.

[7] S. Yoshizawa, "Doppler resilient underwater acoustic communication using stretchable symbols with multiple sequences," WSEAS Transactions on Systems, vol. 24, pp. 548-558, 2025, DOI: 10.37394/23202.2025.24.48.

[8] H. Ren, X. Hu, F. Xu, X. Jun, W. Qing, C. Zhan, Y. Chen, "SNR estimation algorithm of LFM signal based on FRFT for long range and shallow underwater acoustic communication systems," MTS/IEEE OCEANS 2014 - Taipei, Taiwan, pp. 1-6, Apr. 2014, DOI: 10.1109/OCEANS-TAIPEI.2014.6964468.

[9] P. van Walree, "On the definition of receiver output SNR and the probability of bit error," MTS/IEEE OCEANS-Bergen, 2013, pp. 1-9, June 2013, DOI: 10.1109/OCEANS-Bergen.2013.6608087.

[10] G. Qiao, Y. Xiao, L. Wan, X. Guo, H. Jia, "Analysis of SNR metrics for a typical underwater acoustic OFDM system," IEEE

Access, vol. 7, pp. 183565-183579, Dec. 2019, DOI: 10.1109/ACCESS.2019.2960304.

[11] J. Yang, X. Wang, S. Park, H. Kim, "Direct path detection using multipath interference cancellation for communication-based positioning system" EURASIP Journal on Advances in Signal Processing 2012, 188(2012), DOI:10.1186/1687-6180-2012-188.

[12] M. Shin, J. Park, "Implementation of RPL protocol modifications to improve IoT communication performance", WSEAS Transactions on Systems, vol. 24, pp. 403-412, May 2025, DOI:10.37394/23202.2025.24.35.

Contribution of Individual Authors to the Creation of a Scientific Article (Ghostwriting Policy)

The authors equally contributed to the present research, at all stages from the formulation of the problem to the final findings and solution.

Sources of Funding for Research Presented in a Scientific Article or the Scientific Article Itself

No funding was received for conducting this study.

Conflict of Interest

The authors have no conflicts of interest to declare.